Proceedings of the Eighteenth International Conference on
Civil, Structural and Environmental Engineering Computing
Edited by: P. Iványi, J. Kruis and B.H.V. Topping
Civil-Comp Conferences, Volume 10, Paper 2.2
Civil-Comp Press, Edinburgh, United Kingdom, 2025
ISSN: 2753-3239, doi: 10.4203/ccc.10.2.2

Study of the Soil-Structure Interaction on a Portal Frame Railway Bridge Through Experimental Validation

J. Chordà-Monsonís[1], J. C. Sánchez-Quesada[1], E. Moliner[1], A. Romero[2], P. Galvín[2] and M. D. Martínez-Rodrigo[1]

[1] Department of Mechanical Engineering and Construction, Universitat Jaume I, Castelló de la Plana, Spain
[2] Escuela Técnica Superior de Ingeniería, Universidad de Sevilla, Spain

Abstract

Soil-structure interaction plays a major role in the dynamic response of partially-buried structures such as portal frame railway bridges. However, it is seldom included in numerical models, as it usually has associated a high computational cost. However, studies show that this intricate interaction mechanism is a cause of discrepancy between experimental and measured modal parameters, which could induce an erroneous assessment of the serviceability limit states of the structures and uneconomical bridge designs. For this reason, a study on an existing portal frame is conducted in this work. First, the modal parameters are identified from experimental data. Then, a 3D finite-element numerical model considering the track-bridge-soil system is implemented. Perfectly matched layers are used as absorbing boundaries. Dynamic stiffness functions are derived and used to implement a simplified version of the model on which the soil is substituted by a series of frequency-dependent spring-damper el-

ements. The dynamic problem is solved by complex modal superposition to predict the bridge response under operating conditions. Track irregularities are taken into account. The results obtained are satisfactory, allowing to obtain the bridge response with reasonable accuracy and in an efficient manner.

Keywords: vibration, finite elements, experimental measurements, high speed, computational effort, ballasted track.

1 Introduction

Portal frame bridges are a common constructive solution used in railway lines to implement underpass crossings below the tracks. This allows to optimise space and facilitate the implementation of the train infrastructure in a coherent manner. This type of bridge consists of a reinforced concrete rigid frame flanked by integral wing walls. On the sides, its walls are surrounded by an embankment, therefore leaving a major area of the structure in direct contact with the soil. Portal frames are also a recurrent solution because of economical reasons, as they are relatively cheap and are usually executed in a routine fashion. However, given the great number of portal frames in modern railway networks, assessing the main factors that affect their design process is relevant [1]. In this regard, a key aspect is the bridge dynamic performance, that, in this type of bridges, is determined by the soil-structure interaction (SSI) [2]. Although this is well-known, simulating SSI is generally complex and time-consuming. Because of this, SSI is not always included in numerical models aimed at assessing the dynamic performance of railway bridges.

In the case of partially-buried structures such as portal frames, the large contact area with the soil provides a high capacity to dissipate energy, which can affect in a notable way its modal properties and dynamic response under train passages. For this reason, as some authors have pointed out, neglecting the dynamic stiffness of the surrounding soil may induce divergences between numerical and experimental modal parameters [3]. Consequently, this could lead to imprecision when determining the bridge resonant speed and, in the end, to inefficient structural solutions [4, 5]. On the contrary, considering SSI in the numerical simulations could favour a more realistic evaluation of the Serviceability Limit States in the design phase of new bridges and also in the case of existing structures when a change in the traffic conditions is required. Hence, further investigation should be conducted on SSI, as the exact impact of this factor on the bridge dynamic response is still not well known, particularly on this type of structures. This may also be explained by a lack of reliable simple models to simulate SSI in a cost-efficient manner. Apart from that, works including experimental-numerical validation on portal frames are seldom reported in the literature [1].

In view of this, this contribution presents a complete study on an existing portal frame railway bridge with the following objectives: (i) to identify the modal parame-

ters of the bridge from experimental data and (ii) to predict its dynamic response under passing trains in an accurate and efficient manner. To this end, a 3D finite-element (FE) numerical model of the structure is implemented including the track-bridge-soil system. The soil domain is padded with perfectly matched layers (PML) to absorb the radiating soil waves and satisfy Sommerfeld's radiation condition. This full model is used to obtain dynamic stiffness (also called impedance) functions in a subsequent 3D FE simplified model in which the soil is substituted by a series of linear spring-damper elements. Then, the procedure explained in [6] for implementing SSI on beam-type bridges is adapted to the case of the portal frame and its dynamic response under train passages is simulated based on complex modal superposition. Randomly-generated track irregularities are included in the numerical model to assess the rail condition in a more realistic manner. Additionally, the effect of vehicle-bridge interaction (VBI) is introduced as an additional amount of damping, following the Equivalent Additional Damping Approach (EADA) proposed in [7].

2 The portal frame

Located at the kilometric point 31+200 in the high-speed (HS) line Madrid−Sevilla, the *Camino de las Huertas* underpass is a portal frame railway bridge. The bridge deck is a broad structure of 22.1 m width and 8 m span length. The section of the underpass consists of a rectangular integral box of 5.7 m height built with reinforced concrete. The bridge holds three tracks: two for HS services and one for conventional traffic. This condition leads to the most characteristic feature of the portal frame, as it is divided along its width in two sections by means of a longitudinal joint, resulting in two coupled structures: one below the conventional traffic track and another under the HS tracks. Figure 1 shows two images of the portal frame. The bridge dimensions can be seen on Figure 2, where the dashed line represents the longitudinal joint.

Figure 1: The structure under study: (a) the bridge, from the HS side, and (b) a Google Earth satellite image.

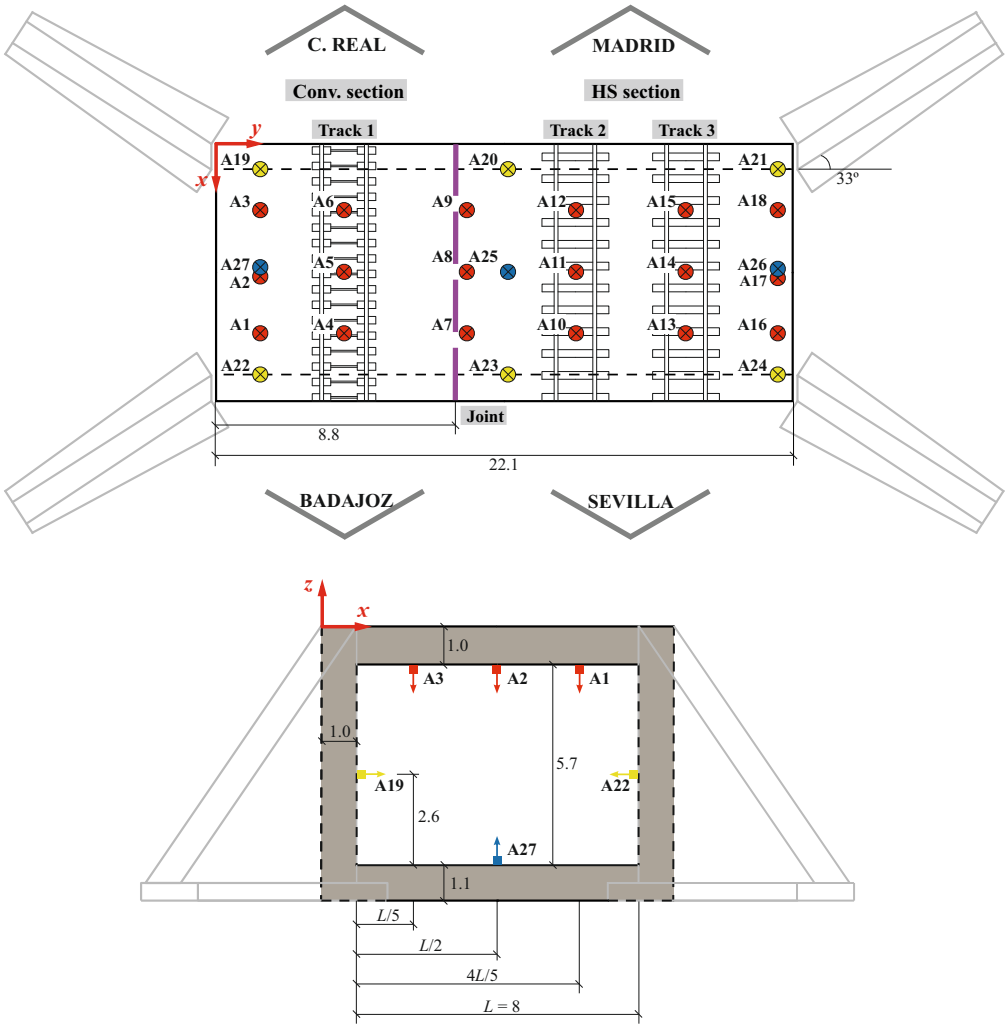

Figure 2: Dimensions of the bridge and accelerometer layout.

3 Modal identification

Data from an experimental program carried out in September 2022 was used to identify the modal parameters of the bridge. 27 piezoelectric accelerometers with nominal sensitivity of 10 V/g were attached on the inner face of the slab, as indicated in Figure 2: 18 on the top slab (shown in red); 6 on the inner side of the vertical walls at 2.6 m high (shown in yellow); and 3 on the floor (shown in blue). The dynamic response of the bridge was recorded under the passage of 27 trains and also under no other excitation than ambient vibration. Data was obtained at a sampling frequency of 4096 Hz and then decimated to 256 Hz. A Chebyshev filter of 1 Hz was applied. Then, an operational modal analysis (OMA) was carried out. The Enhanced Frequency Domain Decomposition method (EFDD) was used to identify the bridge vibration modes. The analysis revealed that the slab decoupling into two distinct structures results in an asymmetric modal behaviour of the underpass, with the HS and conventional bridge sections contributing to the modes in differing proportions. As a result, coupled or mixed modes emerge, exhibiting deformations in both sections. Nevertheless, certain

uncoupled modes are also observed in some instances.

Figure 3 shows the estimated modal parameters of the bridge, where the dashed line represents the longitudinal joint. Among the identified modes, the first mode represents the decoupled longitudinal bending mode of the HS section. The second mode is close in terms of frequency to the next one, however, this mode presents a more pronounced deformation in the HS region. Therefore, the third mode could be identified as the fundamental mode of the conventional section. Mode shapes 4 and 6 stand for particular transverse bending modes of the conventional section, practically decoupled from the rest of the bridge. Finally, the fifth mode presents a predominant transverse deformation of the HS section. In order to estimate modal damping, this parameter is calculated from the free vibrations of the structure left after train passages. This approach is chosen as this situation is more representative of the real behaviour of the bridge under operating conditions in comparison to when it is subjected to ambient vibration [8]. Among the results obtained, high damping ratios are estimated, particularly in the first four modes, which denotes a clear influence of the soil.

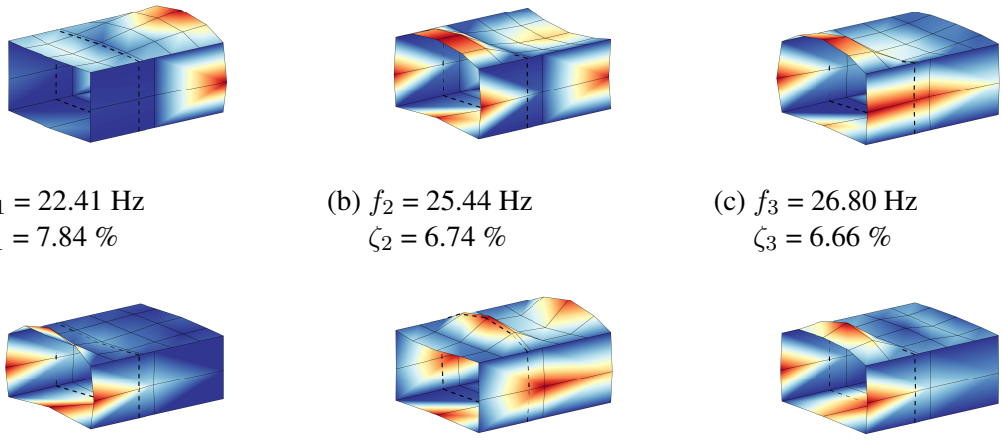

(a) f_1 = 22.41 Hz
ζ_1 = 7.84 %

(b) f_2 = 25.44 Hz
ζ_2 = 6.74 %

(c) f_3 = 26.80 Hz
ζ_3 = 6.66 %

(d) f_4 = 36.23 Hz
ζ_4 = 4.49 %

(e) f_5 = 44.27 Hz
ζ_5 = 3.18 %

(f) f_6 = 55.51 Hz
ζ_6 = 2.52 %

Figure 3: Estimated modal parameters of the portal frame.

4 Numerical approach

This section presents the numerical procedure adopted to simulate the dynamic response of the portal frame while maintaining a reasonable computational cost. To this end, a comprehensive 3D finite element model is developed in the first place, considering the track, the bridge and the surrounding soil. This initial model is used to derive dynamic stiffness functions to model SSI in a subsequent simplified model.

4.1 The full soil-bridge-track interaction model

This model is implemented in ANSYS(R) v.25.1. In it, the tracks, the bridge structure and the soil domain are simulated. To avoid spurious wave reflections at the model boundaries, solid Perfectly Matched Layers (PML) elements are included. This allows to reduce the required soil domain. Soil and PML lengths are determined based on convergence studies as $L_{soil} = 6\,\text{m}$ and $L_{PML} = 0.5\,\text{m}$, as indicated in Figure 4(a). In total, three layers of PML elements are introduced. The meshing in the PML region is discretised to fit between 5 and 20 elements in a single wave length $\lambda = 2\pi \cdot C_s/\omega$, being C_s the shear wave propagation speed of the soil and ω the highest identified natural frequency of the bridge [9]. The entire soil domain is considered homogeneous with $C_s = 350\,\text{m}$. This value is calibrated based on a preliminary calibration step carried out on this model. The soil domain has dimensions of 24 m $\times$ 49.1 m $\times$ 7.5 m. In total, the model has 1,340,132 degrees of freedom (DOF). An image of the model is shown in Figure 4(b). The mechanical properties of the model are listed in Table 1.

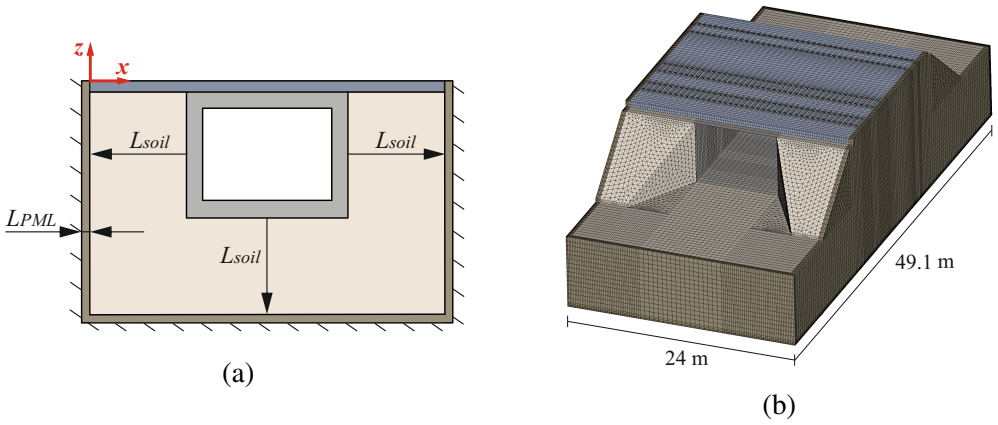

Figure 4: Full track-bridge-soil interaction model: (a) main dimensions, and (b) view of the FE bridge.

4.2 The simplified soil-bridge-track simplified model

This model is implemented based on an inertial decoupling of the track-bridge system from the surrounding soil, which is substituted by a series of discrete linear frequency-dependent spring-dampers that simulate the dynamic interaction of the soil with the portal frame. These elements are arranged along 65 uniformly distributed points over the area of the bridge-soil interface at the bridge walls and the bottom face of the box slab. Three spring-dampers are located at each point, two tangential and one perpendicular to the surface, as indicated in Figure 5(a). This model, shown in Figure 5(b) is implemented with 175,904 DOFs, which constitutes an important reduction in comparison to the previous case.

Entity	Part	Property	Symbol	Value	Unit
Track	Rail	Elastic Modulus	E_r	$2.10 \cdot 10^{11}$	Pa
		Moment of inertia	I_r	$3038 \cdot 10^{-8}$	m^4
		Linear mass	m_r	60.34	kg/m
	Rail pad	Stiffness	K_d	$1.00 \cdot 10^{8}$	N/m
		Damping	C_d	$7.50 \cdot 10^{4}$	Ns/m
	Sleepers	Elastic modulus	E_p	$3.60 \cdot 10^{10}$	Pa
		Poisson's ratio	ν_p	0.2	[-]
		Mass	m_p	320	kg
	Ballast	Elastic modulus	E_b	$1.10 \cdot 10^{8}$	Pa
		Poisson's ratio	ν_b	0.2	[-]
		Density	ρ_b	1950	kg
		Height	h_b	0.728	m
Bridge	Slab	Elastic modulus	E_l	$35.71 \cdot 10^{9}$	Pa
		Poisson's ratio	ν_l	0.2	[-]
		Density	ρ_l	2500	[-]
	Joint	Elastic modulus	E_j	9522.50	Pa
		Poisson's ratio	ν_j	0.2	[-]
		Density	ρ_j	2500	[-]
Soil	Whole domain	Shear wave speed	c_s	350	m/s
		Poisson's ration	ν_s	0.2	[-]
		Density	ρ_s	1950	kg/m^3

Table 1: Mechanical properties of the model.

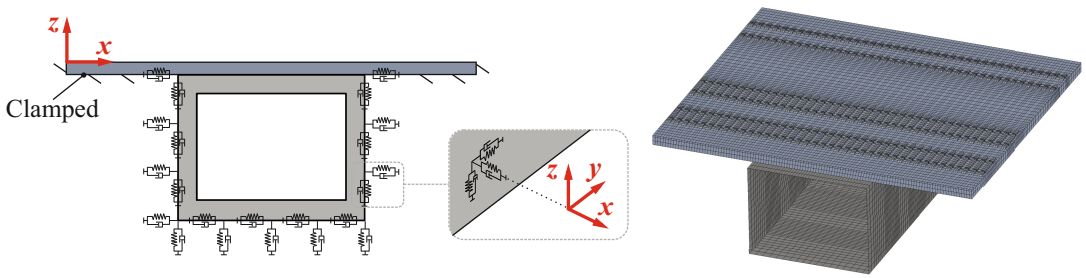

(a) (b)

Figure 5: Simplified track-bridge-soil interaction model: (a) schematic front view, and (b) view of the FE discretisation.

4.3 SSI implementation

The SSI is first evaluated on the full model. To do so, a harmonic analysis is conducted considering a distributed vertical force $F_s(\omega)$ on both rails of track 2 along the bridge span. At each point on which a spring-damper will be attached, the dynamic stiffness can be calculated as the ratio between the resultant input force and the point displacement in the corresponding direction: $K_{v,d}(\omega) = F_s(\omega)/U_s(\omega)$, obtaining the following properties of stiffness $K_v(\omega) = \text{Re}[K_{v,d}(\omega)]$ and damping $C_v(\omega) = \text{Im}[K_{v,d}(\omega)]/\omega$ for each spring-damper element [6]. In this work, the spring-dampers are tuned to the fundamental frequency of the bridge f_1.

To finalise the process, a subsequent calibration step is carried out on the mechanical properties of the bridge, focusing specifically on the ballast density and the elastic modulus of the bridge slab. Given the asymmetric modal behaviour of the portal frame, it is found necessary to differentiate the mechanical properties of the two bridge sections to achieve a close match with the experimental modal parameters. In this sense, the ballast density of the HS and conventional sections is set to 2340 and 1560 kg/m^3, respectively. On the other hand, the elastic modulus of the slab is calibrated as 30.35 and 26.07 GPa, respectively. Then, a modal analysis is conducted, leading the results in Table 2, where the experimental and numerical bridge frequencies are compared. The Modal Assurance Criterion (MAC) is used to assess similarity between pairs.

Results	f_1	f_2	f_3	f_4	f_5	f_6
Exp.	22.41	25.44	26.80	36.23	44.27	55.51
Num.	22.49	25.43	27.01	34.15	37.51	63.57
MAC	0.63	0.56	0.63	0.71	0.77	0.81

Table 2: Experimental and numerical bridge frequencies (in Hz) and MACs.

5 Solution to the dynamic problem

This section addresses the formulation of the dynamic problem, which is solved by means of complex modal superposition. To this aim, mode shapes are computed with ANSYS and then are exported to MATLAB. Subsequently, the following calculations are conducted.

5.1 The SSI interaction problem

The equilibrium equation of the system, applied to the bridge model containing N DOFs with initial conditions of displacement $\boldsymbol{u}(0) = \boldsymbol{u}_0$ and velocity $\dot{\boldsymbol{u}}(0) = \dot{\boldsymbol{u}}_0$, is:

$$\boldsymbol{M}\ddot{\boldsymbol{u}}\left(t\right)+\boldsymbol{C}\dot{\boldsymbol{u}}\left(t\right)+\boldsymbol{K}\boldsymbol{u}\left(t\right)=\boldsymbol{F}\left(t\right) \tag{1}$$

where $\boldsymbol{M}$, $\boldsymbol{C}$ and $\boldsymbol{K}$ are the mass, damping and stiffness matrices. Due to the damping introduced by the spring-damper elements, the damping in the system is non-proportional. As a result, mode shapes are complex and the position of each DOF is defined by amplitude and phase. Thus, a set of $2N$ equations is required to evaluate the solution of the N DOFs of the structure, that can be written from Eq. 1 as a first order differential matrix equation:

$$\boldsymbol{A}\dot{\boldsymbol{y}}\left(t\right)+\boldsymbol{B}\boldsymbol{y}\left(t\right)=\boldsymbol{P}\left(t\right) \tag{2}$$

where:

$$\boldsymbol{A}=\begin{bmatrix}\boldsymbol{C} & \boldsymbol{M}\\ \boldsymbol{M} & \boldsymbol{0}\end{bmatrix}\quad \boldsymbol{B}=\begin{bmatrix}\boldsymbol{K} & \boldsymbol{0}\\ \boldsymbol{0} & -\boldsymbol{M}\end{bmatrix}\quad \boldsymbol{P}=\begin{bmatrix}\boldsymbol{F}(t)\\ \boldsymbol{0}\end{bmatrix}\quad \boldsymbol{y}(t)=\begin{bmatrix}\boldsymbol{u}(t)\\ \dot{\boldsymbol{u}}(t)\end{bmatrix} \tag{3}$$

being $\boldsymbol{y}$ the state vector and $\boldsymbol{A}$ and $\boldsymbol{B}$ two real and symmetric matrices of dimensions $2N\times 2N$. In the free vibration case, Eq. 2 yields $\boldsymbol{A}\dot{\boldsymbol{y}}\left(t\right)+\boldsymbol{B}\boldsymbol{y}\left(t\right)=\boldsymbol{0}$. The trial solution can be obtained as $\boldsymbol{y}(t)=\boldsymbol{\Psi}_j e^{s_j t}$, where s_j is the j-th element of a total set $2N$ eigenvalues and Ψ_j is the corresponding eigenvector:

$$\boldsymbol{\Psi}_j=\begin{bmatrix}\boldsymbol{\phi}_j\\ s_j\boldsymbol{\phi}_j\end{bmatrix} \tag{4}$$

Then, natural frequencies, damped natural frequencies and modal damping ratios are determined from the eigenvalues as $\omega_j=|s_j|$, $\omega_{dj}=|\mathrm{Im}[s_j]|$ and $\zeta_j=-\mathrm{Re}[s_j]/|s_j|$, respectively. The solution to Eq. 2 can be expressed as:

$$\boldsymbol{y}(t)=\sum_{j=1}^{2N}\boldsymbol{\Psi}_j z_j(t) \tag{5}$$

Taking into account the orthogonality conditions $\boldsymbol{\Psi}_j^T\boldsymbol{A}\boldsymbol{\Psi}_k=0$ and $\boldsymbol{\Psi}_j^T\boldsymbol{B}\boldsymbol{\Psi}_k=0$ for any pair of modes $j\neq k$ (where the superscript T indicates matrix transpose) and normalising the eigenvectors to the matrix $\boldsymbol{A}$ (i.e., $\boldsymbol{\Psi}_j^T\boldsymbol{A}\boldsymbol{\Psi}_j=1$), Eq. 2 results into a set of $2N$ uncoupled equations [6], where $p_j(t)=\boldsymbol{\Psi}_j^T\boldsymbol{P}(t)$:

$$\dot{z}_j(t)+\alpha_j z_j(t)=p_j(t) \tag{6}$$

This is a non-stiff differential equation that can be addressed numerically. In this work, this equation is solved by means of a Runge Kutta (4,5) explicit algorithm. Then, the bridge displacements are calculated through complex modal superposition, as indicated below. This expression takes into account that eigenvalues and eigenvectors appear as pairs of complex conjugates.

$$\mathbf{u}(t) = \sum_{j=1}^{N} 2\text{Re}[\boldsymbol{\phi}_j z_j(t)] \tag{7}$$

5.2 Mode shapes normalisation

To proceed as in the previous section, mode shapes obtained with ANSYS (normalised by default to the mass matrix $\mathbf{M}$) need to be normalised to the $\mathbf{A}$ matrix when exported to MATLAB. To this aim, a scaling parameter allowing to perform this operation is derived below. Initially, mode shapes normalised to the mass matrix (as indicated by the M superscript) fullfill that $\boldsymbol{\Psi}_j^{T,M}\mathbf{A}\boldsymbol{\Psi}_j^{M} \neq 1$. Taking into account Equations 3 and 4, and further developing the previous condition, it can be expressed as:

$$\boldsymbol{\Psi}_j^{T,M}\mathbf{A}\boldsymbol{\Psi}_j^{M} = \begin{bmatrix} \boldsymbol{\phi}_j \\ s_j\boldsymbol{\phi}_j \end{bmatrix}^{T,M} \begin{bmatrix} \mathbf{C} & \mathbf{M} \\ \mathbf{M} & \mathbf{0} \end{bmatrix} \begin{bmatrix} \boldsymbol{\phi}_j \\ s_j\boldsymbol{\phi}_j \end{bmatrix}^{M} = \boldsymbol{\phi}_j^{T,M}\mathbf{C}\boldsymbol{\phi}_j^{M} + 2m_j s_j \tag{8}$$

where m_j is the modal mass. Additionally, because of orthogonality, modes satisfy $\boldsymbol{\Psi}_j^{T,M}\mathbf{A}\boldsymbol{\Psi}_k^{M} = 0$ for any mode $j \neq k$, from which it can be derived that $\boldsymbol{\phi}_j^{T,M}\mathbf{C}\boldsymbol{\phi}_k^{M} = -(s_j + s_k)\boldsymbol{\phi}_j^{T,M}\mathbf{M}\boldsymbol{\phi}_k^{M}$. As eigenvalues appear as pairs of complex conjugates ($s_k = \bar{s_j}$), and knowing that $\omega_j = |s_j|$ and $\zeta_j = -\text{Re}[s_j]/|s_j|$, the precedent expression can be rewritten accordingly:

$$\boldsymbol{\phi}_j^{T,M}\mathbf{C}\bar{\boldsymbol{\phi}}_j^{M} = 2m_j\zeta_j\omega_j \tag{9}$$

Now, Equation 9 is used to approximate the term $\boldsymbol{\phi}_j^{T,M}\mathbf{C}\boldsymbol{\phi}_j^{M}$ in Equation 8 by assuming that $\boldsymbol{\phi}_j^{T,M}\mathbf{C}\bar{\boldsymbol{\phi}}_j^{M} \approx \boldsymbol{\phi}_j^{T,M}\mathbf{C}\boldsymbol{\phi}_j^{M}$. As the modal mass equals 1 due to mass normalisation, Equation 8 results into:

$$\boldsymbol{\Psi}_j^{T,M}\mathbf{A}\boldsymbol{\Psi}_j^{M} = 2m_j\zeta_j\omega_j + 2m_j s_j = 2(\omega_j\zeta_j + s_j) = \delta_j \tag{10}$$

where δ_j is the scaling parameter that allows to adapt the normalisation of the modal shapes from $\mathbf{M}$ to $\mathbf{A}$:

$$\boldsymbol{\Psi}_j = \boldsymbol{\Psi}_j^{M}/\sqrt{\delta_j} \tag{11}$$

Similarly, modes comply with $\boldsymbol{\Psi}_j^{T,M}\mathbf{B}\boldsymbol{\Psi}_k^{M} = 0$ because of orthogonality conditions. This leads to $\boldsymbol{\phi}_j^{T,M}\mathbf{K}\bar{\boldsymbol{\phi}}_j^{M} \approx \boldsymbol{\phi}_j^{T,M}\mathbf{K}\boldsymbol{\phi}_j^{M} \approx \omega_j^2$ considering the previous approach. Then, further developing the expression $\boldsymbol{\Psi}_j^{T}\mathbf{B}\boldsymbol{\Psi}_j = \alpha_j$ while scaling as indicated in Equation 11 allows to obtain $\alpha_j = (\omega_j^2 - s_j^2)/\delta_j$, which can be used in Equation 5 to solve the dynamic problem. Eventually, the bridge modes are normalised with this procedure and used to compute the solution as per Equation 6.

5.3 Quasi-static and dynamic loads

Three excitation mechanisms are considered: a quasi-static contribution, a parametric excitation and a dynamic loading. The quasi-static contribution is modelled as a series of moving forces travelling at a constant speed, therefore neglecting the inertial effects of the vehicle. Then, the parametric excitation is induced by the moving loads circulating along rails discretely supported at each sleeper. Lastly, the dynamic loading includes the effect of track irregularities, which are modelled based on a stationary Gaussian random process characterised by its one-sided power spectral density function (PSD) based on ISO 8606, as $S(\kappa_x) = S(\kappa_{x0})(\kappa_x/\kappa_{x0})^{-w}$ with $\kappa_{x0} = 1$ rad/m, $w = 3.5$, and the sampling wave-number κ_x defined in steps of $\Delta\kappa_x = \pi/V$ rad/m in the interval between the bogie passing frequency of the train divided by its travelling speed ($f_{pb}/V \cdot 2\pi = 2\pi/d$, where d is the characteristic distance of the train) and the ratio between the highest frequency of the bridge and the train velocity ($f_{max} \cdot 2\pi/V$). Finally, a minor degree of track deterioration is assumed with $S(\kappa_{x0}) = 1 \times 10^{-9}$ m^3 [10]. Subsequently, random unevenness profile samples $r(x)$ are generated as a superposition of harmonic functions with aleatory phase angles:

$$r(x) = \sum_{n=1}^{Np} \sqrt{2\, S(\kappa_x)\Delta\kappa}\cos(\,\kappa_x x - \varphi_n) \tag{12}$$

where N_p is the number of points, κ_x is the sampling wave-number, $\Delta\kappa_x$ is the wave-number step and φ_n are the random phase angles uniformly distributed in the interval [0, 2π]. Next, the irregularity profile is used to approximate the vehicle-track interaction force $F_{v/t}$ as a result of the track unevenness, as shown in Equation 13:

$$F_{v/t}(x,\omega) = m_w \cdot \frac{d^2 r(x)}{dt^2} + K_{d,t}(\omega) \cdot r(x) \tag{13}$$

where m_w is the vehicle unsprung mass and $K_{d,t}(\omega)$ the track dynamic stiffness. This parameter is estimated from a harmonic analysis performed using the full track-bridge-soil interaction model. It considers two identical concentrated forces, $F_{r1}(\omega)$ and $F_{r2}(\omega)$, at midspan. Each load acts on one rail of the track. Then, the rail displacements at the points where the forces are being applied are obtained as $U_{r1}(\omega)$ and $U_{r2}(\omega)$. Finally, the track dynamic stiffness is computed as $K_{d,t}(\omega) = 1/2 \cdot [(F_{r1}(\omega) + F_{r2}(\omega))/(U_{r1}(\omega) + U_{r2}(\omega))]$. In a first approach, it is assumed that $K_{d,t}(\omega)$ at midspan is representative for the totality of the track length. In an analogous way to the calibration of the spring-dampers, $K_{d,t}(\omega)$ is admitted constant and equal to the value attained at f_1.

5.4 Additional damping

To obtain a more realistic prediction of the structural performance, the VBI benefit may be approximated if an additional amount of damping ζ_{tot} is introduced in the system. In this work, this quantity is determined as $\zeta_{tot} = \zeta_b + \Delta\zeta_{\text{EADA}}$. ζ_b is the

structural damping of the bridge and is obtained based on the Eurocode criterion for pre-stressed concrete bridges [11]. On the other hand, $\Delta\zeta_{\text{EADA}}$ is the supplementary damping ratio proposed by Yau et al. [7]. This ratio is calculated based on the relationship between the modal properties of the train and the bridge. Eventually, ζ_{tot} is introduced in the system through each eigenvalue s_j under consideration, leading to the subsequent modified eigenvalues $s_{jd} = -(\zeta_j + \zeta_{\text{Total}})|s_j| + \text{Im}[s_j]i$. Then, the dynamic load problem is solved as previously explained.

6 Response under train passages

The dynamic response of the portal frame is calculated under the passage of the RENFE S103 train, which circulated in track 3 from Sevilla to Madrid at 228 km/h. This conventional train has eight coaches and two driven passenger cars. As indicated in Figure 6, its characteristic distance is 24.775 m. More information about it can be found in Reference [12]. With respect to the additional damping introduced to simulate this passage, $\zeta_{tot} = 2.77$ with $\zeta_b = 1.84$ and $\Delta\zeta_{\text{EADA}} = 0.93$. Below, Figure 7 shows the bridge vertical acceleration response in the time and in the frequency domains. The experimental register is depicted in black. The case including the quasi-static contribution (denoted as Q) and the track irregularities (denoted as I) is shown in dark red colour. Apart from that, the light red curves represent the numerical response when, in addition to the previous considerations, the additional damping ratio ζ_{tot} is also included. Finally, the numerical response considering only the quasi-static contribution and the additional damping is shown in blue. The data is filtered applying Chebyshev filters with high-pass and low-pass frequencies of 1 and 30 Hz, respectively. The experimental acceleration is extracted from sensor A15.

As Figure 7 suggests, a good approximation is attained in the cases where track irregularities are considered. In contrast, when only the quasi-static contribution is computed, the prediction for frequencies higher than 15 Hz underestimates the measured bridge acceleration. This highlights the relevance of simulating this excitation mechanism to replicate the bridge behaviour at higher frequencies, as they contribute to incrementing the bridge response. The effect of the additional damping is also noticeable, particularly at the highest acceleration peaks in the frequency domain.

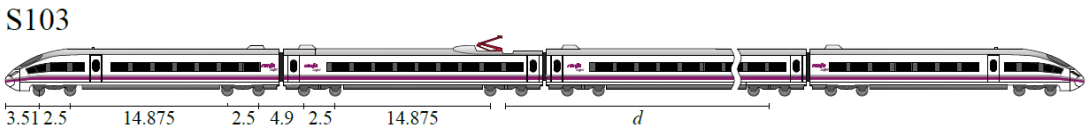

Figure 6: Scheme of axles of the train Siemens S103.

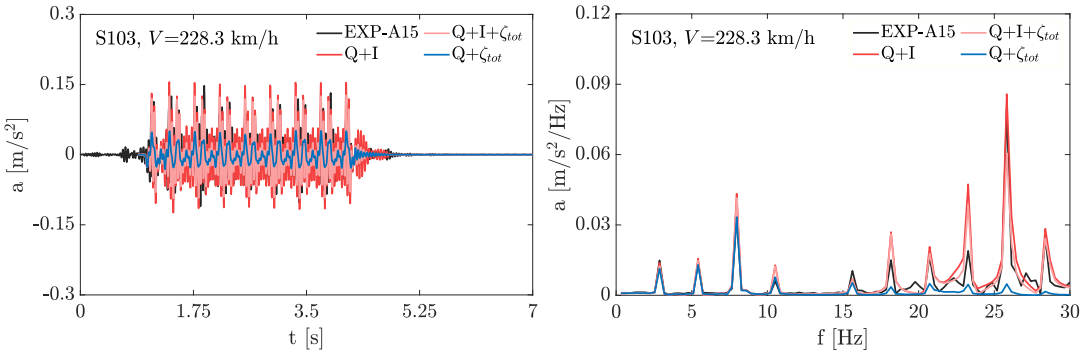

Figure 7: Comparison of the vertical acceleration in the time and frequency domains.

7 Conclusions

In this contribution, a procedure to simulate SSI in an efficient manner is presented and applied to the case of an existing portal frame. To this aim, first, SSI is evaluated on a soil-track-bridge interaction model to obtain dynamic stiffness functions that substitute the soil in a subsequent simplified version of it. Then, the dynamic problem with non-proportional damping is addressed and solved by means of complex modal superposition [6]. The conclusions of this contribution can be derived as follows:

- The modal identification process was key to understand the modal behaviour of the bridge and in the design phase of the model. In particular, differentiating the mechanical properties of the HS and the conventional section was important for replicating the real conditions of the structure.

- The proposed numerical approach has been successfully implemented. The formulation enables an efficient solution of the dynamic SSI problem. Moreover, the approach used to approximate the normalisation of the mode shapes could be useful in similar cases.

- The results of the moving load analysis are satisfactory when track irregularities are taken into account. Therefore, it can be concluded that the proposed SSI modelling procedure provides a reliable estimation of the bridge response under passing trains. Besides, the final results are achieved without incurring in an excessive computational cost.

- In the present work, the dynamic excitation due to track irregularities is introduced in an estimated way. However, the final results reflect the importance of considering this excitation mechanism, as it has significantly improved the prediction of the bridge response at frequencies higher than 15 Hz in comparison to the case where only the quasi-static contribution is considered. Also, the additional damping has been practical to provide a more realistic bridge prediction in certain frequency peaks close to the structural modes of the portal frame.

Acknowledgements

The authors acknowledge the financial support provided by the Universitat Jaume I through the contract (PREDOC/2022/26) and the grant (E-2023-08), the Spanish Ministry of Science (PID2022–138674OB–C2), Andalusian Ministry of University, Research and Innovation (PROYEXCEL 00659) and Andalusian Scientific Computing Centre.

This project has received funding from the Europe's Rail Joint Undertaking under Horizon Europe research and innovation programme under grant agreement No. 101121765 (HORIZON-ER-JU-2022-ExplR-02). Views and opinions expressed are however those of the author(s) only and do not necessarily reflect those of the European Union or Europe's Rail Joint Undertaking. Neither the European Union nor the granting authority can be held responsible for them.

References

[1] J. Vega, A. Fraile, E. Alarcon, L. Hermanns, "Dynamic response of underpasses for high-speed train lines", Journal of Sound and Vibration, 331, 5125-5140, 2012.

[2] A. Zangeneh, C. Svedholm, A. Andersson, C. Pacoste, "Identification of soil-structure interaction effect in a portal frame railway bridge through full-scale dynamic testing", Engineering Structures, 159, 299-309, 2018.

[3] A. Zangeneh, S. François, G. Lombaert, C. Pacoste, "Modal analysis of coupled soil-structure systems", Soil Dynamics and Earthquake Engineering, 144, 106645, 2021.

[4] M.D. Martínez-Rodrigo, P. Galvín, A. Doménech, A. Romero, "Effect of soil properties on the dynamic response of simply-supported bridges under railway traffic through coupled boundary element finite element analyises", Engineering Structures, 170, 78-90, 2018.

[5] P. Salcher, "Effect of soil-structure interaction on the dynamics of portal frame railway bridges", Bautechnik, 97(7), 490-498, 2020.

[6] P. Galvín, A. Romero, E. Moliner, E. Connolly, M.D. Martínez-Rodrigo, "Fast simulation of railway bridge dynamics accounting for soil-structure interaction", Bulletin of Earthquake Engineering, 23, 3195-3213, 2022.

[7] J. Yau, M.D. Martínez-Rodrigo, A. Doménech, "An additional damping approach to assess vehicle-bridge interaction for train-induced vibration of short-span railway bridges", Engineering Structures, 188, 469-479, 2019.

[8] P. Galvín, A. Romero, E. Moliner, G. De Roeck, M.D. Martínez-Rodrigo, "On the dynamic characterisation of railway bridges through experimental testing", Engineering Structures, 226, 111261, 2021.

[9] C. Coronado, N. Gidwani, E. Moliner, "Calculation of dynamic impedance foundations using finite element procedures", San Francisco, Bechtel Power Corporation Nuclear Security and Environmental Edition, 2016.

[10] G. Lombaert, G. Degrande, J. Kogut, S. Fran¸cois, "The experimental validation of a numerical model for the prediction of railway induced vibrations", Journal of Sound and Vibration 297, 512–535, 2006.

[11] CEN, EN 1991-2, Eurocode 1: Actions on Structures - Part 2: Traffic loads on bridges and other civil engineering works, European Committee for Standardization (CEN), Brussels, 2023.

[12] J.C. Sánchez-Quesada, E. Moliner, A. Romero, P. Galvín, M.D. Martínez-Rodrigo, "Train-track-bridge interaction effects on highly skewed girder bridges of short-to-medium spans for increasing operating speeds", Structure and Infrastructure Engineering, 1–25, 2024.